


Personalized neoantigen vaccine combined with PD-1 blockade increases CD8⁺ tissue-resident memory T-cell infiltration in preclinical hepatocellular carcinoma models

Hengkai Chen,^{1,2,3,4} Zhenli Li,^{1,2,3} Liman Qiu,^{1,2,3} Xiuqing Dong,^{1,2,3} Geng Chen,^{1,2,3} Yingjun Shi,^{1,2,3} Linsheng Cai,^{1,2,3} Wenhan Liu,^{1,2,3} Honghao Ye,^{1,2,3} Yang Zhou,^{1,2,3} Jiahe Ouyang,^{1,2,3} Zhixiong Cai,^{1,2,3} Xiaolong Liu ^{1,2,3}

To cite: Chen H, Li Z, Qiu L, *et al.* Personalized neoantigen vaccine combined with PD-1 blockade increases CD8⁺ tissue-resident memory T-cell infiltration in preclinical hepatocellular carcinoma models. *Journal for ImmunoTherapy of Cancer* 2022;**10**:e004389. doi:10.1136/jitc-2021-004389

► Additional supplemental material is published online only. To view, please visit the journal online (<http://dx.doi.org/10.1136/jitc-2021-004389>).

HC and ZL contributed equally.

Accepted 30 August 2022



© Author(s) (or their employer(s)) 2022. Re-use permitted under CC BY-NC. No commercial re-use. See rights and permissions. Published by BMJ.

For numbered affiliations see end of article.

Correspondence to

Professor Xiaolong Liu;
xiaolong.liu@gmail.com

Professor Zhixiong Cai;
caizhixiong1985@163.com

ABSTRACT

Background Personalized neoantigen vaccine could induce a robust antitumor immune response in multiple cancers, whose efficacy could be further enhanced by combining with programmed cell death 1 blockade (α -PD-1). However, the corresponding immune response and synergistic mechanisms remain largely unclear. Here, we aimed to develop clinically available combinational therapeutic strategy and further explore its potential antitumor mechanisms in hepatocellular carcinoma (HCC).

Methods Neoantigen peptide vaccine (NeoVAC) for murine HCC cell line Hepa1-6 was developed and optimized by neoantigen screening and adjuvant optimization. Then the synergistic efficacy and related molecular mechanisms of NeoVAC combined with α -PD-1 in HCC were evaluated by orthotopic HCC mouse model, single-cell RNA sequencing, tetramer flow cytometry, immunofluorescence, etc. The tumor-killing capacity of CD8⁺ tissue-resident memory T cells (CD8⁺ T_{RMS}) was assessed by orthotopic HCC mouse model, and autologous patient-derived cells.

Results NeoVAC, which consisted of seven high immunogenic neoantigen peptides and clinical-grade Poly(I:C), could generate a strong antitumor immune response in HCC mouse models. Significantly, its efficacy could be further improved by combining with α -PD-1, with 80% of durable tumor regression and long-term immune memory in orthotopic HCC models. Moreover, in-depth analysis of the tumor immune microenvironment showed that the percentage of CD8⁺ T_{RMS} was remarkably increased in NeoVAC plus α -PD-1 treatment group, and positively associated with the antitumor efficacy. In vitro and in vivo T-cell cytotoxicity assay further confirmed the strong tumor-killing capacity of CD8⁺ T_{RMS} sorting from orthotopic mouse HCC or patient's HCC tissue.

Conclusions This study showed that NeoVAC plus α -PD-1 could induce a strong antitumor response and long-term tumor-specific immune memory in HCC by increasing CD8⁺ T_{RMS} infiltration, which might serve as a potential immune-therapeutic target for HCC.

INTRODUCTION

Hepatocellular carcinoma (HCC) is the third leading cause of cancer-related death worldwide.¹ Despite great progress has been made in current treatment strategies, such as surgery, transcatheter arterial chemoembolization (TACE) and targeted therapy, the 5-year overall survival (OS) in patients with advanced HCC is still less than 20% over the past decades.² Lately, immune checkpoint blockade immunotherapies based on anti-programmed cell death 1 (PD-1) and anti-programmed cell death ligand 1 (PD-L1) antibodies have shown great antitumor activity in patients with advanced HCC, with a clinical responses rate of 14–31% in several clinical trials.³ However, there are still a considerable number of patients with HCC who cannot benefit from anti-PD-1 monotherapy due to restricted tumor infiltrating lymphocytes (TILs).⁴ Thus, there is an urgent need to develop novel strategies for increasing tumor-specific T-cell infiltration and improving efficacy of immunotherapy in HCC.

Neoantigens, which are derived from non-synonymous mutations, incomplete splicing, translation of alternatives, or post-translational modifications, can potentially be presented on the surface of tumor cells by major histocompatibility complex (MHC) molecules and be recognized as neoepitopes by T cells, and thus become attractive targets for T-cell-mediated immune responses.^{5–7} Neoantigen candidates are mainly derived from non-synonymous somatic variants in cancer cells, which could be identified by genomic and transcriptomic sequencing. It has been reported that personalized neoantigen-based cancer therapeutic vaccine

could induce the infiltration of neoepitope-specific T cells into tumor tissue to kill cancer cells expressing these antigens.^{5–8} Recent clinical trials also have highlighted the safety, feasibility and immunogenicity of personalized neoantigen vaccines in patients with both hypermutated or non-hypermutated cancers, such as melanoma and glioma.^{5–10} HCC is considered as an inflammation-related immunogenic tumor with strong immune-suppressed microenvironment, moderated tumor mutation burden (median number of 5 Mut/Mb), as well as relatively poor infiltration of TILs. Others' and our previous studies have shown that neoantigen burden could well reflect patients with HCC prognosis and some of them could serve as an excellent target for HCC immunotherapy.^{11–13} However, whether neoantigen-based vaccine could elicit robust antitumor immune responses in advanced HCC still needs to be deeply explored.

Based on the fact that mono-immunotherapy in patients with advanced HCC is prone to produce drug resistance and lead to poor efficacy,¹⁴ several trials are exploring to combine different treatment strategies in HCC such as anti-vascular endothelial growth factor (VEGF) plus PD-1 blockade (α -PD-1) and cytotoxic T lymphocyte-associated antigen-4 blockade plus α -PD-1. Nevertheless, almost all these combinational therapies would significantly increase related serious toxicities and side effects (ranging from 12% to 38% of patients), while the objective remission rate (ORR) of patients with advanced HCC remains limited due to that the efficacy of immune checkpoint blockade relies on pre-existing of tumor-specific TILs.^{15–18} Therefore, it is an urgent need to develop new combinational treatment strategies for HCC with precision targeting, high treatment efficacy and low side effects. Considering the broad landscape of personalized neoantigen vaccines in generating neoantigen-specific T cells, it is reasonable to hypothesize that personalized NeoVAC and α -PD-1 combinational therapy could improve the ORR and durability of immune therapy in HCC by generating more tumor-specific T cells. Hu *et al* have demonstrated that patients who have undergone personalized NEOVAC treatment further receiving α -PD-1 therapy could achieve better therapeutic effects in melanoma.¹⁹ Of note, a large phase Ib clinical trial of combining personalized NeoVAC (NEO-PV-01) with α -PD-1, in patients with advanced melanoma, non-small cell lung cancer, and bladder cancer (NCT02897765) also showed durable neoantigen-specific T-cell reactivity with 59%, 39%, 27% ORR rate, respectively, and without treatment-related serious adverse events simultaneously.²⁰ These results suggest that NeoVAC combined with α -PD-1 therapy might be a safe and effective combination strategy clinically. However, the efficacy and synergistic mechanisms of this combination strategy for HCC and its corresponding impact on tumor microenvironment (TME) remain largely unclear.

Here, we developed and optimized a personalized neoantigen peptide vaccine (NeoVAC) for murine HCC cell line, to evaluate its safety, feasibility and efficacy in

murine HCC models. Meanwhile, we further designed an NeoVAC/ α -PD-1 combination therapy strategy to achieve a favorable long-term outcome in murine orthotopic HCC model. Moreover, comprehensive analysis of tumor immune microenvironment dynamics and potential anti-tumor immune responses after combination therapy was performed. In general, our study provides solid evidences for personalized neoantigen therapy plus α -PD-1 in HCC treatment, and revealed potential function and mechanisms of tissue-resident memory T cells (CD8⁺ T_{RMS}), which could be available as a potential immune-therapeutic target in future HCC immunotherapy.

MATERIALS AND METHODS

Neoantigen identification and immunogenicity validation

DNA and RNA extracted from murine HCC cell line Hepa1-6 cells and C57BL/6 mouse tail tissue were subjected to whole exome sequencing and transcriptomic sequencing. Mutation variants of Hepa1-6 cells were called using VarScan²¹ software with mouse genome mm10 as reference and only mutations with variant allele frequency >10% and depth more than 20× were retained. Remaining variants were annotated with wANNOVAR²² to filter non-synonymous mutations.

Immunogenicity of all mutations was evaluated using NetMHCpan²³ binding affinity predictor, and mutations that produce 9-mer mutant peptides with IC₅₀<500 nM to H-2K^b allele were considered as candidate neoantigens. The detailed methods were shown in online supplemental methods.

Neoantigen immunogenicity validation

Male C57BL/6 mice (6–8 weeks old) were purchased from China Wushi (Shanghai, China). To identify potential neoantigen peptides, 26 neoantigen mutations from Hepa1-6 cells were selected and 20 of them were successfully synthesized for long peptides (17 amino acids in length) by the standard solid-phase synthetic peptide chemistry (>95% purity, Genscript Biotechnology, China). For neoantigen immunogenicity validation, 20 neoantigen peptides were randomly divided into two pools (2 μ g/peptide) and mixed with 50 μ g Poly(I:C) (Guangdong South China Pharmaceutical); then, the mixture was used to subcutaneously immunize male C57BL/6 mice at the lateral flank on day 0, day 4 and day 8, respectively. Afterwards, the mice were sacrificed on day 14 and the splenic T cells were counted for ELISPOT assay. The detailed methods were shown in online supplemental methods.

In vivo antitumor efficacy evaluation

Subcutaneous HCC model and orthotopic HCC model were constructed by injecting 3×10⁶ Hepa1-6 cells into the armpits of mice and inoculating with 3×10⁵ Hepa1-6-luc cells mixed with the matrigel plugs at liver subcapsular of mice for 10 days, respectively.

For NeoVAC optimization and combinational treatment, the subcutaneous HCC model and/or the orthotopic HCC model were randomly divided into 4–10 groups ($n=5$) as indicated and then subcutaneously injected with identified neoantigen peptides ($2\mu\text{g}/\text{peptide}$) mixed with each adjuvant (Pam3CSK4, Poly(I:C), Mpl, Flagellin, R848, CpG ODN) or Poly(I:C) alone in $200\mu\text{L}$ volume on day 0, day 4 and day 8, respectively. The $\alpha\text{-PD-1}$ (BioLegend, 124328) was injected intravenously ($50\mu\text{g}$ per mouse). The mice treated with phosphate buffered saline (PBS) were used as control. Tumor burden was monitored every 3 days in subcutaneous HCC model by vernier caliper and every 10 days in orthotopic HCC model by IVIS Spectrum animal imaging system (PerkinElmer, USA). For recurrence/metastasis rechallenge experiments, all mice were injected with 1×10^5 Hepa1-6-luc cells orthotopically again 10 days after being cured by NeoVAC plus $\alpha\text{-PD-1}$ treatment and injected with 2×10^6 Hepa1-6-luc cells via tail vein on day 50 after first treatment. Naive mice were included as the control. Tumor burden was similarly monitored every 10 days as mentioned above. Therapeutic efficacy, tissue processing, flow cytometry, tetramer staining and sequencing, immunofluorescence, immunohistochemistry (IHC) and H&E staining were shown in online supplemental methods. The gating strategies of flow cytometry analysis in this study were illustrated in online supplemental figure S1.

Single-cell RNA sequencing library construction and bulk RNA sequencing data analysis

CD45^+ T cells were sorted from HCC tumor in orthotopic HCC model treated with neoantigen and/or $\alpha\text{-PD-1}$ by fluorescence-activated cell sorting (FACS) and subjected to single-cell RNA sequencing (scRNA-seq) library preparation by using the 10x Genomics Chromium Single Cell 5' Library & Gel Bead reagent kit and Chromium Single Cell V(D)J Enrichment Kit. The scRNA-seq reads acquired from 10x Genomics platform were aligned using Cell Ranger (V.5.0.1, 10x Genomics) to reference genome (mm10) with default parameters. After mapping, qualified unique molecular identifier (UMI) reads and cells were further filtered with Seurat (V.4.0.3)²⁴ in R (V.4.1.0).

After removing low-quality cells and likely doublets, 5900 cells of each group were randomly selected and included for following analysis. Then the gene expression levels were normalized using the NormalizeData function with the LogNormalize method. The t-distributed stochastic neighbor embedding (t-SNE) dimensionality reduction was conducted and Seurat functions FindNeighbors and FindClusters were used for cell clustering. Then cell clusters were annotated by SingleR package (V.1.6.1)²⁵ using the annotation from combining Immgen data set²⁶ and MouseRNAseq data set. Those detailed methods and other analyses including single-cell V(D)J analysis, CD8^+ T-cell development trajectory, cell–cell interaction analysis and bulk RNA-seq data analysis were shown in online supplemental methods.

In vitro and in vivo T-cell cytotoxicity assay

$\text{CD8}^+\text{CD69}^-/\text{CD8}^+\text{CD69}^+$ T cells were sorted from fresh tumor excisions of orthotopic HCC model treated with NeoVAC plus $\alpha\text{-PD-1}$ and patients with HCC. Detailed methods for T-cell cytotoxicity assay in vitro were shown in online supplemental methods. For in vivo T-cell cytotoxicity assay, the $\text{CD8}^+\text{CD69}^-$ T cells or $\text{CD8}^+\text{CD69}^+$ T cells (2×10^5 per mouse) were intravenously injected into orthotopic HCC model ($n=4$), respectively. The mice in orthotopic HCC model mice treated with PBS were taken as control. Then all treated animals received daily injections of 1×10^3 IU interleukin (IL)-2 infusion for 5 days. The tumor burden was monitored every 5 days similarly as mentioned above.

Statistical analysis

Pearson's correlation coefficient was used to evaluate the correlation matrices. Survival curves were generated using Kaplan-Meier estimates and the p values were examined using the log-rank test. Sample data were compared using a two-tailed Student's t-test or one-way analysis of variance by the GraphPad Prism V.8.0 software, $*p<0.05$ was set as statistically significant. $**p<0.01$, $***p<0.001$, $****p<0.001$. All the data were shown as means \pm SD/SEM through at least three biologically independent samples.

RESULTS

Neoantigen screening and identification in murine HCC cell line

To screen the potential neoantigen peptides in murine HCC cell line Hepa1-6 cells, DNA and RNA extracted from Hepa1-6 cells were subjected to whole exome sequencing and RNA-seq, respectively, and further analyzed by bioinformatics algorithms (figure 1A). As shown in figure 1B, 8009 qualified non-synonymous mutations were identified in whole exome sequence data by VarScan (variant allele frequency $\geq 10\%$, sequencing depth ≥ 20 , online supplemental table S1); and RNA-seq data confirmed that 278 of those non-synonymous mutations were steadily expressed (variant allele frequency $\geq 10\%$, depth ≥ 20 and transcripts per million of corresponding gene ≥ 1). To further identify possibly immunogenic neoantigens, binding affinity between mutated peptides and MHC molecules (Hepa1-6 cells and C57BL/6 mice: H-2K^b allele) was predicted by NetMHCpan, showing that 26 mutations had high affinity (binding affinity value: $\text{IC}_{50}<500\text{ nM}$) with H-2K^b allele (online supplemental table S2). Then, the mutated long peptides (17aa) of 20 neoantigens with potential high immunogenicity ($\text{IC}_{50}<500\text{ nM}$ to H-2K^b) were successfully synthesized for preparing NeoVAC. After that, 20 neoantigen peptides were randomly divided into two groups, and further mixed with Poly(I:C) to subcutaneously immunize the male C57BL/6 mice at the lateral flank on day 0, day 4 and day 8, respectively. Afterwards, the mice were sacrificed 14 days after the initial injection, and the splenic T

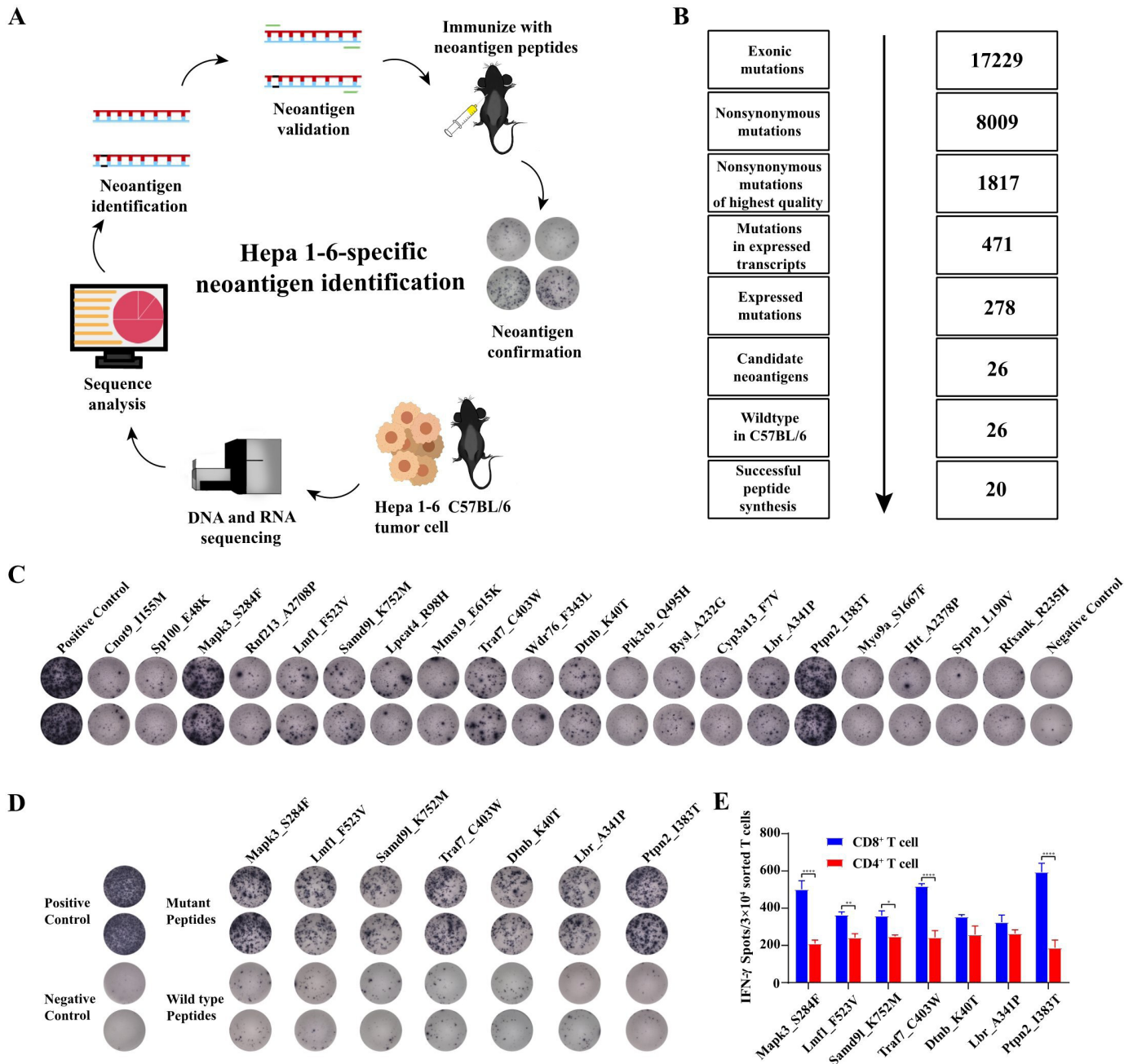


Figure 1 Neoantigen identification and immunogenicity validation. (A) Tumor neoepitope identification processes for murine hepatocellular carcinoma cell line Hepa1-6 cells. (B) Screening workflow of neoantigen peptides. (C) Potential neoantigen immunogenicity validation performed by ELISPOT. (D) Cross-reactivity analysis between seven identified neoantigen peptides and corresponding wild-type peptides. (E) Potential neoantigen immunogenicity analysis of seven identified neoantigen peptides in sorted splenic CD4⁺ and CD8⁺ T cells. Results are shown as mean±SD. **p*<0.05; ***p*<0.01; ****p*<0.001; *****p*<0.0001. IFN, interferon.

cells were isolated for immunologic testing. Ex vivo interferon (IFN)- γ ELISPOT assay revealed that 7 out of 20 mutation-coding peptides (Mapk3_S284F, Lmf1_F523V, Samd91_K752M, Traf7_C403W, Dtnb_K40T, Lbr_A341P, Ptpn2_I383T) could elicit significant immune responses in immunized mice by using autologous splenic T cells stimulated by each neoantigen peptide-pulsed autologous matured dendritic cells (DCs) and without cross-reactivity against the corresponding wild-type peptide (figure 1C,D). To further

explore which T-cell subsets were activated by those seven neoantigen peptides, the CD4⁺ or CD8⁺ T cells were sorted from the spleen in immunized mice. The results showed that DCs could activate both CD4⁺ or CD8⁺ T cells by presenting these seven neoantigen peptides. Among them, five neoantigen peptides (Mapk3_S284F, Lmf1_F523V, Samd91_K752M, Traf7_C403W, Ptpn2_I383T) were mainly presented to CD8⁺ T cells via H-2K^b (figure 1E and online supplemental figure S2). Accordingly, those seven peptides with

obvious immune response *in vivo* were used as hepa1-6 NeoVAC components for downstream studies.

NeoVAC optimization

Due to the weak immunogenicity of peptide vaccine, it needs to combine with the corresponding adjuvant to initiate both innate and adaptive immune signals for inducing sufficient T-cell activation and protective immune responses. Toll-like receptors (TLRs) are a typical type of pattern recognition receptors expressed on the surface of a variety of cells, which can recognize the molecular patterns of pathogens or foreign substances. There are six TLR agonists that have been shown to elicit robust immune responses in clinical trials, including TLR1/2 agonist Pam3csk4, TLR3 agonist Poly(I:C), TLR5 agonist

Flagellin, TLR7/8 agonist resiquimod (R848) and TLR9 agonist CpG oligodeoxynucleotide (CpG ODN).^{27–36}

To optimize the antitumor immune responses induced by those TLR agonists combined with our peptide vaccine, subcutaneous HCC model was constructed and then vaccinated with NeoVAC containing those seven neoantigen peptides (2 µg/peptide) plus each TLR agonist (Pam3csk4, Poly(I:C), Mpla, Flagellin, R848 and CpG ODN) at day 0, 4 and 8, respectively (figure 2A). As shown in figure 2B, after 24 days from receiving neoantigen vaccination, significant tumor regression was observed in the groups with treatment of five TLR agonists (Pam3csk4, Poly(I:C), Mpla, Flagellin and R848) when compared with the negative control or neoantigen peptide alone. Significantly, among those five TLR agonists, we found

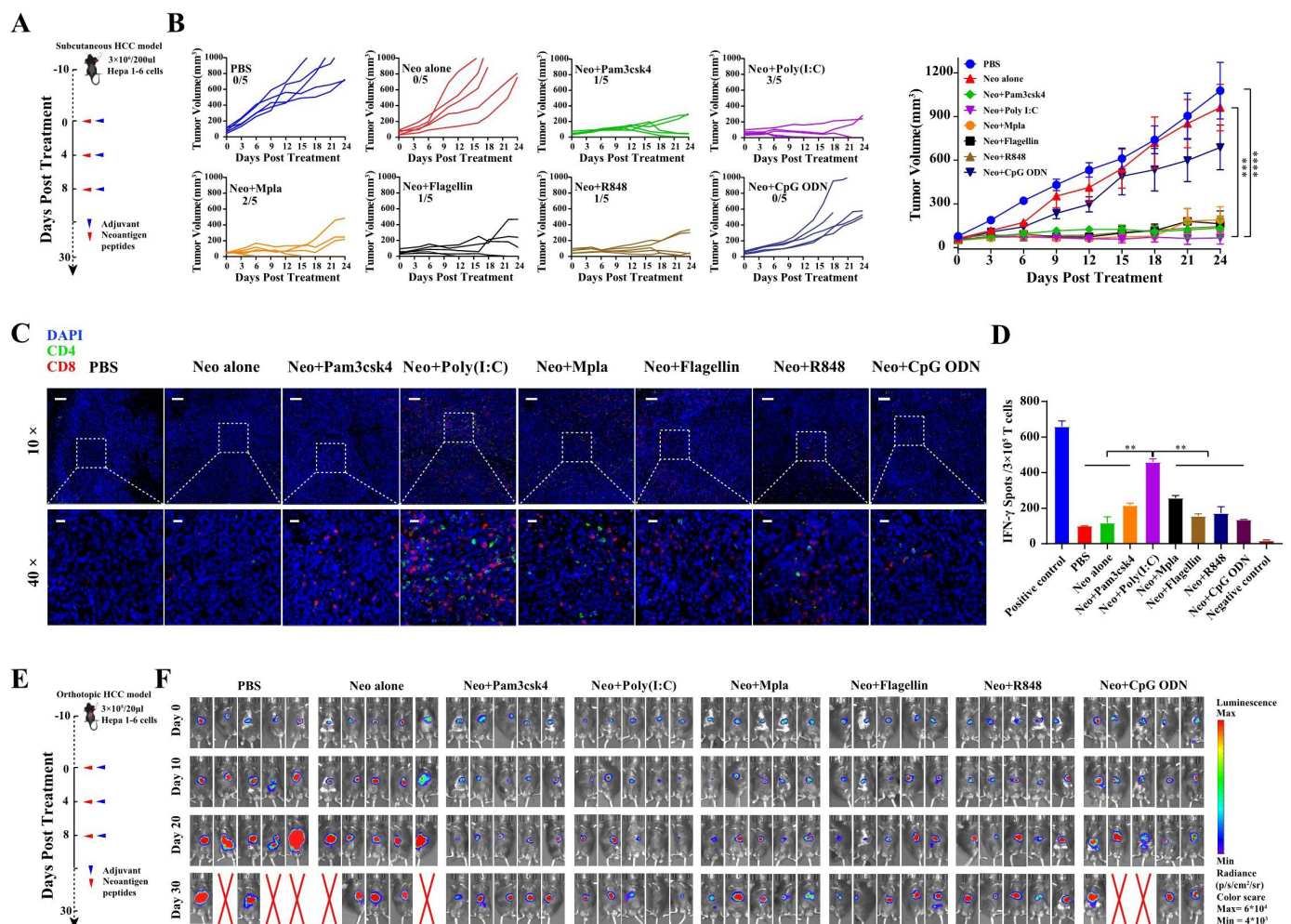


Figure 2 Adjuvant optimization for neoantigen peptide vaccine NeoVAC preparation. (A) Schematic representation of the vaccination schedule for screening adjuvant in subcutaneous HCC model. (B) Tumor growth curves of each group (n=5) treated with neoantigen peptides pulsed with different Toll-like receptor agonists as adjuvant (Pam3csk4, Poly(I:C), Mpla, Flagellin, R848 and CpG-ODN). Results are shown as mean ± SEM. (C) The representative immunofluorescence image of CD4⁺ and CD8⁺ T-cell infiltration in tumor tissues at each treated group. Scale bars, 100 µm (10×), 40 µm (40×). (D) The histogram of ELISPOT assay showing neoantigen-specific reactivity of splenic T cells against the pool of seven neoantigen peptides. Results are shown as mean ± SD. (E) Schematic representation of the vaccination schedule for screening adjuvant in orthotopic HCC model. (F) Tumor burden monitoring of each group (n=5) treated with neoantigen peptides pulsed with different adjuvant by bioluminescence imaging. Neo, neoantigen peptides. The statistical analysis was performed with analysis of variance analysis. *p<0.05; **p<0.01; ***p<0.001; ****p<0.0001. HCC, hepatocellular carcinoma; IFN, interferon; PBS, phosphate buffered saline.

that Poly(I:C) as vaccine adjuvant was significantly better than other four adjuvants (Pam3csk4, Flagellin and R848,1/5; Mpl, 2/5), with 60% (3/5) of the mice's tumors completely abrogated. Then, we further evaluated the immune infiltration of TILs in tumor tissue using immunofluorescence staining. As expected, the result revealed that the infiltration of both CD8⁺ and CD4⁺ T cells was obviously increased in neoantigen peptides plus Poly(I:C) group when compared with other groups (figure 2C). Moreover, ELISPOT assay confirmed that the neoantigen-specific reactivity of splenic T cells against seven neoantigen peptides was significantly higher in neoantigen peptides plus Poly(I:C) group than that in other treated groups (figure 2D and online supplemental figure S3A). While the immunogenicity to the selected neoepitopes could not be detected when mice were treated with Poly(I:C) alone (online supplemental figure S3B). Meanwhile, to better reveal the real antitumor efficacy of neoantigen vaccines, orthotopic HCC model was further constructed for vaccinating with corresponding neoantigen vaccines containing those seven neoantigen peptides plus each TLR agonist as the same as in the subcutaneous HCC model (figure 2E). Significantly, as shown in figure 2F and online supplemental figure S3C, the neoantigen peptides mixed with Poly(I:C) showed the best antitumor efficacy among all adjuvants, with 60% (3/5) of the mice maintaining relatively low tumor burden on day 30 (figure 2F and online supplemental figure S3C). Taken together, these results indicated that Poly(I:C) could serve as an optimal adjuvant for NeoVAC preparation in HCC treatment.

Moreover, to further investigate whether those seven neoantigen peptides were all required for antitumor response, each neoantigen peptide or all seven peptides were mixed with 50 µg Poly(I:C) to vaccinate the orthotopic HCC mice model following above mentioned schedule, respectively (online supplemental figure S4A). Compared with PBS or Poly(I:C)-treated group, the single neoantigen peptide mixed with Poly(I:C)-treated group showed a certain delay of tumor growth; however, as expected, the NeoVAC containing all seven neoantigen peptides showed the strongest antitumor efficacy (online supplemental figure S4B,C).

Meanwhile, we also found that the NeoVAC treatment alone could not completely inhibit tumor growth, which might be due to immune escape induced by the immunosuppressive TME. Therefore, we further analyzed the expression of PD-1 in TILs and PD-L1 in tumor tissues in NeoVAC-treated mice. Flow cytometry analysis showed that, in NeoVAC-treated mice, TILs displayed high expression of PD-1 (online supplemental figure S5A). Correspondingly, PD-L1 was also obviously upregulated in tumor tissues of NeoVAC-treated mice, which was confirmed by IHC analysis (online supplemental figure S5B). Such phenomena suggested an underlying resistance mechanism that limited the efficacy of NeoVAC monotherapy, which could be potentially rescuable by α-PD-1.

Combining NeoVAC with α-PD-1 enhances the antitumor immunity in orthotopic HCC models

Due to the upregulation of PD-1 and PD-L1 following NeoVAC vaccination, we sought to improve antitumor immune response by combining NeoVAC with α-PD-1. As shown in figure 3A, the orthotopic HCC mice were divided into four groups and received PBS, NeoVAC alone, α-PD-1 alone and NeoVAC plus α-PD-1 treatment on days 0, 4, 8 with two independent repeated experiments, respectively. According to the tumor progression profiles shown in figure 3B and online supplemental figure S6A, the tumor burdens in PBS-treated group showed a rapid increase over 20 days and all mice (10/10) were dead on day 60, while 20% and 40% of durable tumor regression were observed in the NeoVAC treated mice and the α-PD-1 treated mice, respectively. Most significantly, the tumor growth of NeoVAC plus α-PD-1 treated mice showed most dramatic tumor suppression with 80% of durable tumor regression when compared with other three treated groups. At the end of the experiments or at the time of mice died spontaneously, the tumors were removed and weighted. Consistent with the bioluminescence images, the tumor weight and H&E staining further confirmed the antitumor efficiency of NeoVAC/α-PD-1 combinational therapy (online supplemental figure 6B,C). Kaplan-Meier analysis further indicated that mice with NeoVAC plus α-PD-1 treatment had significantly longer OS than those treated with PBS, NeoVAC or α-PD-1 alone ($p < 0.0001$, figure 3C). Additionally, we also evaluated the safety of this combination therapy by biochemical tests and H&E staining of organ sections on day 12 after treatment (online supplemental figure S7A–N) and monitoring the body weight change every 3 days (online supplemental figure S7O). These results supported the safety and feasibility of NeoVAC plus α-PD-1 treatment in HCC.

To characterize potential neoantigen-specific immune responses in mice with combination therapy, we further evaluated the status of distinct immune cell phenotypes including matured DCs (CD11c⁺) in lymph nodes (LNs), central memory CD8⁺ T cells (T_{CMs}, CD44⁺ and CD62L⁺) in spleen and the neoantigen neoantigen-specific T cells in tumor tissue obtained on day 12 after receiving combination therapy. Flow cytometry analysis showed that the percentages of matured DCs and CD8⁺ T_{CMs} in the mice with combination therapy were significantly higher than that in other three treated groups (figure 3D and E and online supplemental figure S8A,B). Meanwhile, the neoantigen-specific reactivity of splenic T cells against neoantigen pools by ELISPOT analysis showed that a higher number of IFN-γ spots were observed in the mice with combination therapy when compared with other treated groups (figure 3F). Correspondingly, the percentages of splenic T cells expressing exhaustion marker PD-1 and activation marker 4-1BB were also upregulated after neoantigen restimulation in the mice with combination therapy (figure 3G).

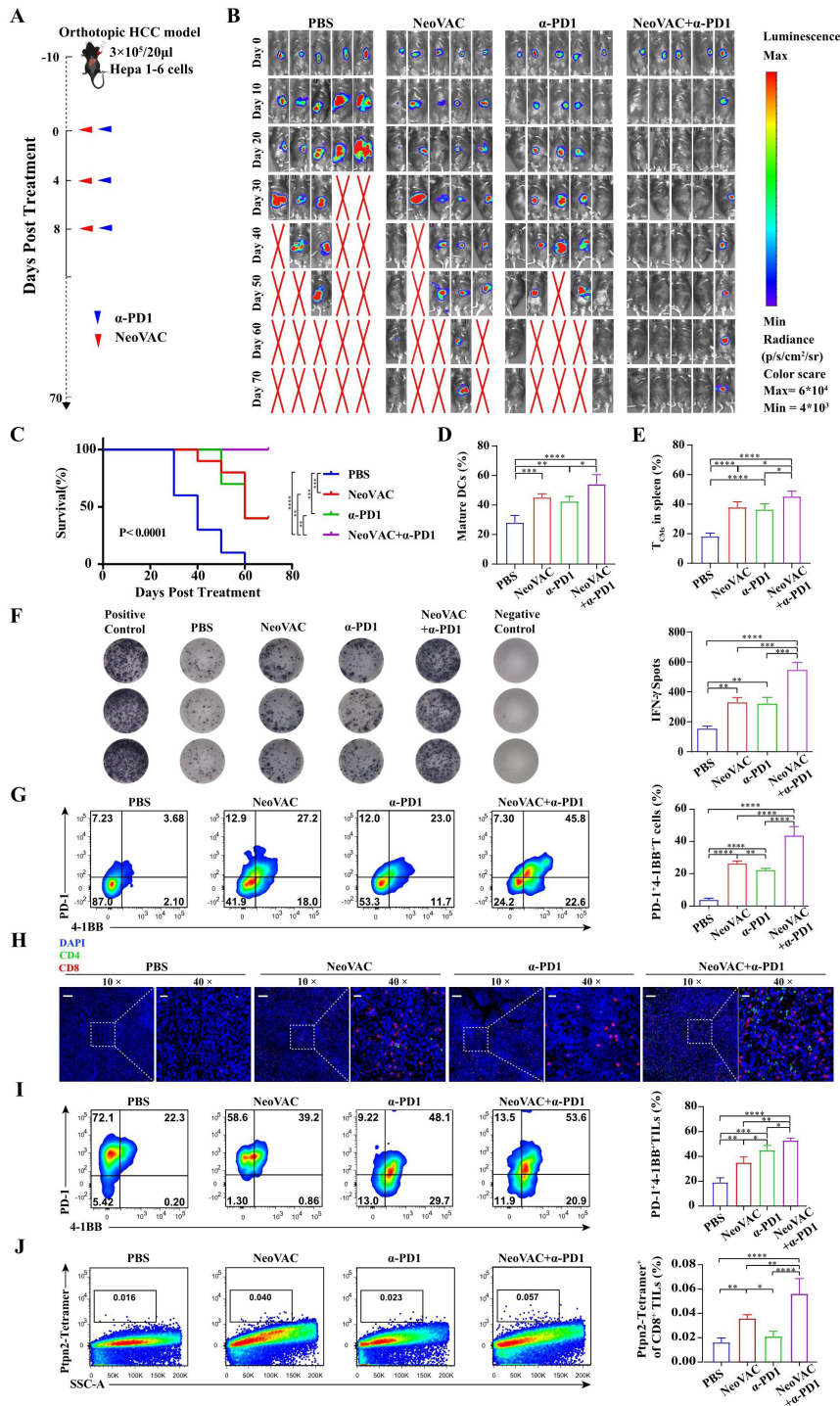


Figure 3 Antitumor efficacy of NeoVAC plus α -PD-1 treatment in orthotopic HCC model. (A) Treatment timeline for NeoVAC plus α -PD-1 treatment in orthotopic HCC model. (B) Tumor burden monitoring of PBS, NeoVAC alone, α -PD-1 alone and NeoVAC plus α -PD-1 treated mice by bioluminescence imaging (n=5). (C) Kaplan-Meier survival curves of PBS, NeoVAC alone, α -PD-1 alone and NeoVAC plus α -PD-1 treated groups (n=10). (D) Flow cytometry showing the percentage of matured DCs (n=5). (E) Flow cytometry showing the percentage of central memory T cells in spleen (n=5). (F) ELISPOT assay showing neoantigen-specific reactivity of splenic T cells against seven neoantigen peptides (n=3). (G) Flow cytometry showing the percentage of CD8⁺ T cells expressing PD-1 and 4-1BB in ELISPOT assay (n=3). (H) The representative immunofluorescence image of CD4⁺ and CD8⁺ T-cell infiltration in tumor tissues. Scale bars, 100 μ m (10 \times), 40 μ m (40 \times). (I) Flow cytometry showing the percentage of infiltrating CD8⁺ T cells expressing PD-1 and 4-1BB (n=3). (J) Flow cytometry analysis showing the percentage of Ptpn2³⁷⁶⁻³⁸⁴ (RWLYWQPTL):H-2K^b specific CD8⁺ T cells in infiltrating CD8⁺ T cells (n=3). Ptpn2, Ptpn2³⁷⁶⁻³⁸⁴:H-2K^b. The statistical analysis was performed with analysis of variance analysis. Survival curves were generated using Kaplan-Meier estimates and tested using the log-rank test. Results are shown as mean \pm SD. *p<0.05; **p<0.01; ***p<0.001; ****p<0.0001. HCC, hepatocellular carcinoma; IFN, interferon; NeoVAC, neoantigen peptide vaccine; PBS, phosphate buffered saline; PD-1, programmed cell death 1; α -PD-1, PD-1 blockade.

Next, we assessed the infiltration of TILs on day 12 by immunofluorescence staining after the mice treated with NeoVAC plus α -PD-1. Unsurprisingly, the result revealed that the infiltration of both CD8⁺ and CD4⁺ T cells was significantly increased in NeoVAC plus α -PD-1 group when compared with other groups (figure 3H). Moreover, flow cytometry analysis of disaggregated TILs isolated from NeoVAC plus α -PD-1 treated-mice showed higher activation marker of 4-1BB expression on CD8⁺ T cells, than the TILs isolated from NeoVAC-treated alone mice (figure 3I), suggesting that a large repertoire of TILs were activated after combination therapy. We further generated a fluorescently labeled tetramer for the strongest immunogenic neoantigen peptide Ptpn2₃₇₆₋₃₈₄ (RWLYWQPTL):H-2Kb (Ptpn2) to detect T cells that expressed Ptpn2-specific T-cell receptors (TCRs) in the TILs. As shown in figure 3J and online supplemental figure S8C, peptide-MHC tetramer staining revealed a statistically significant increase of intratumoral Ptpn2-specific CD8⁺ T cells in NeoVAC alone/plus α -PD-1 treated mice when compared with PBS or α -PD-1 treated mice, which suggested that combination therapy could induce significantly stronger neoantigen-specific T-cell infiltration in tumor. Overall, these results indicated that combined NeoVAC with α -PD-1 could successfully induce a strong neoantigen-specific antitumor response in vivo for HCC treatment.

Combining NeoVAC with α -PD-1 induces long-term memory for preventing HCC recurrence and metastasis

Encouraged by the above results, we further evaluated the tumor prevention efficacy induced by NeoVAC plus α -PD-1 for HCC recurrence and metastasis. As shown in figure 4A, orthotopic tumor-bearing mice were first constructed and received combinational therapy or PBS as previously described, and the tumor burden was measured by bioluminescence imaging. Significantly, 10 days after treatment, tumor burden in all mice (n=6) treated with NeoVAC plus α -PD-1 were all with tumor regression, while PBS treated mice (n=5) still suffered from rapid tumor growth (figure 4B). This result further confirmed the efficacy of combinational therapy in HCC treatment. Next, all cured mice with combinational therapy were orthotopically injected with 1×10^5 Hepa1-6 cells in the liver again (naive mice served as control) to simulate HCC recurrence on day 20 after treatment (figure 4A). It was interesting that the tumor could not grow in five of six cured mice. On contrary, tumor burden of all naive mice underwent a relatively rapid growth (figure 4B). Moreover, we further simulated HCC metastasis in the remaining five mice from combinational therapy by injecting 2×10^6 Hepa1-6 cells via tail vein on day 50 after treatment and new naive mice (n=5) were also served as the control correspondingly (figure 4A). As expected, all mice (5/5) from combinational therapy still could resist metastasis rechallenge on day 90 after treatment while all naive mice occurred severe metastasis (figure 4B).

Furthermore, peptide-MHC tetramer staining revealed that Ptpn2-specific CD8⁺ T cells could be detected in the peripheral blood mononuclear cells collected from combinational therapy treated mice at day 2 after recurrence rechallenge and further significantly upregulated at day 2 after metastasis rechallenge, but only very low level was detected in correspondingly naive mice (figure 4C and online supplemental figure S9A). Remarkably, ELISPOT analysis showed that the splenic T cells collected from combinational therapy treated mice at day 90 after treatment still showed significant sensitivity against neoantigen pools (figure 4D and online supplemental figure S9B). Taken together, these findings suggested that combining NeoVAC with α -PD-1 could induce long-term neoantigen-specific immune memory effects for preventing HCC recurrence and metastasis.

Tumor immune microenvironment changing dynamics during combinational therapy

To further gain insight into the immune microenvironment change of orthotopic HCC models after combinational therapy, sorted CD45⁺ tumor-infiltrating cells from groups including PBS, NeoVAC alone, α -PD-1 alone and NeoVAC plus α -PD-1 treatment were subjected to scRNA-seq and single-cell V(D)J sequencing. Following quality control, a total of 11,007, 8424, 7351 and 5982 cells were retained for those four treated groups, respectively. Then, 5900 cells of each group were randomly selected to gain an intuitive comparison and visualization for following analysis. Using the t-SNE method, a total of 15 cell clusters were identified, including 3 T-cell clusters, 6 monocyte clusters, 2 granulocyte clusters, 2 macrophage clusters, 1 B cell cluster, 1 endothelial cluster and 1 natural killer cell cluster (figure 5A). Among them, two T-cell clusters (C1 and C2) and endothelial cell cluster (C6) were enriched in cells from NeoVAC plus α -PD-1 treated mice while their proportion was relatively limited in PBS-group (figure 5A). As T cells play a major role in antitumor responses induced by NeoVAC or α -PD-1, we further focused on the enriched T-cell clusters. To further dissect the variability within the T-cell compartment, the two enriched T-cell clusters (C1 and C2) were extracted and reclustered, resulting in seven CD8⁺ T-cell clusters and eight CD4⁺ T-cell clusters (figure 5B). We found that the T13 cluster was a subcluster of CD8⁺ T cells mainly from NeoVAC and α -PD-1 treated group but was very limited in the other three groups (figure 5C and online supplemental figure S10A), which were further confirmed by alluvial plot of TCR analysis (figure 5D). Extracting the marker genes of T13 cluster showed an enrichment of Cd69, Ccl4 and Ifng genes, suggesting that T13 represent CD8⁺ T_{RMS} (figure 5E).³⁷ Besides Ifng, T13 cluster also expressed a relatively high level of Gzmb and Tnf, all of which were the canonical cytotoxic mediators produced by CD8⁺ T_{RMS}.³⁸ Consistently, gene set variation analysis of T13 cluster revealed a significant enrichment of genes response to α and γ IFN proteins (online supplemental

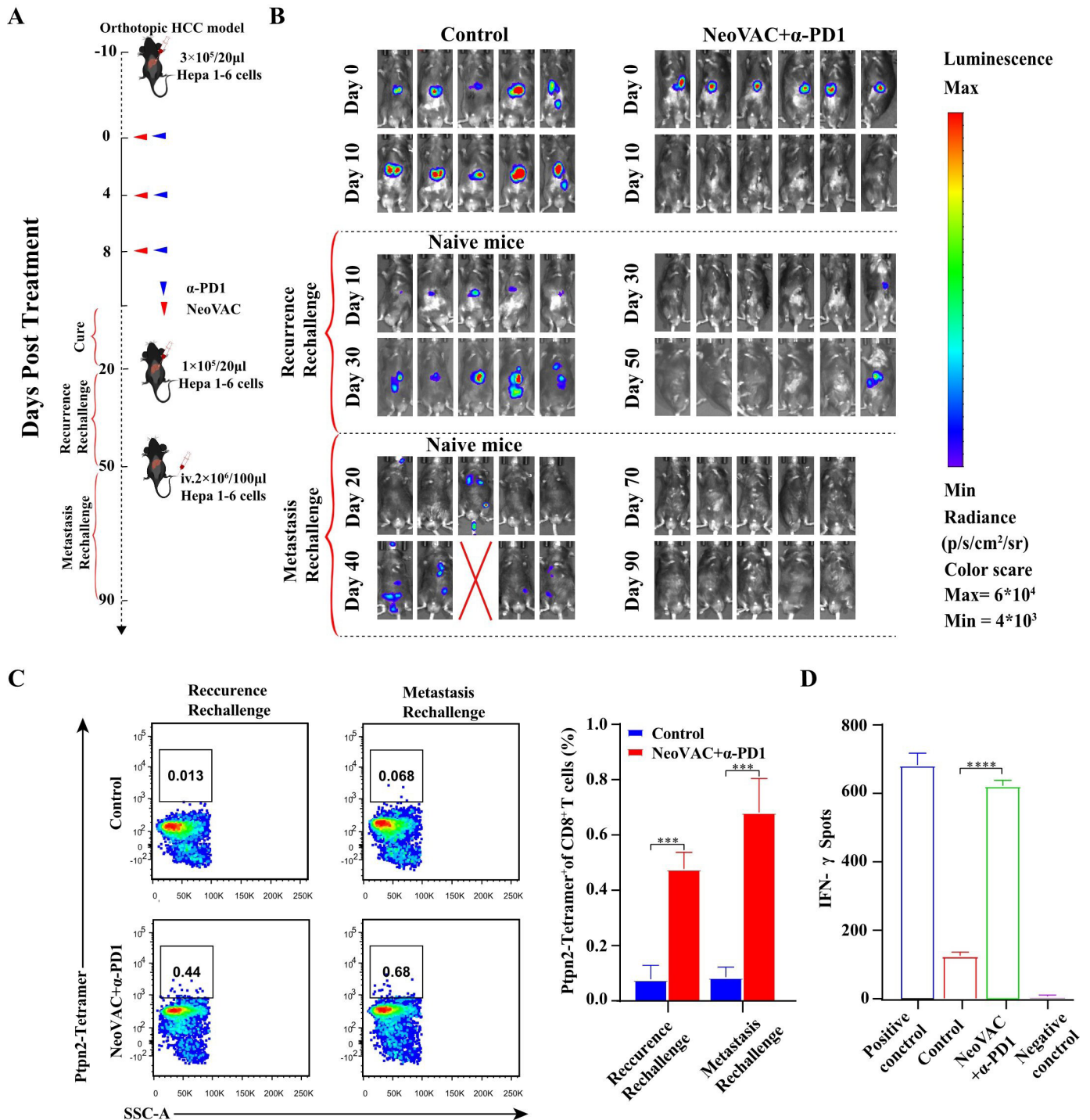


Figure 4 Orthotopic recurrence and metastasis rechallenge of NeoVAC plus α -PD-1 treatment in vivo. (A) Schematic diagram showing the process of establishing orthotopic recurrence and metastasis rechallenge models. (B) Tumor burdens of NeoVAC plus α -PD-1 treated mice ($n=6$) and naive mice ($n=5$) after treatment and rechallenge measured by bioluminescence imaging. (C) Flow cytometry analysis showing the percentage of Ptpn2₃₇₆₋₃₈₄:H-2K^b specific CD8⁺ T cells in blood after 2 days orthotopic recurrence and metastasis rechallenge ($n=3$). (D) ELISPOT assay showing neoantigen-specific reactivity of splenic T cells against seven neoantigen peptides on day 90 after treatment ($n=3$). Ptpn2, Ptpn2₃₇₆₋₃₈₄:H-2K^b. The statistical analysis was performed with analysis of variance analysis. Results are shown as mean \pm SD. * $p<0.05$; ** $p<0.01$; *** $p<0.001$; **** $p<0.0001$. HCC, hepatocellular carcinoma; NeoVAC, neoantigen peptide vaccine; α -PD-1, programmed cell death 1 blockade.

figure S10B), confirming the important roles of CD8⁺ T_{RMS} involved in anticancer immunity.

Additionally, we applied the Monocle 2 algorithm to perform pseudotime analysis and found two evolution

fates of CD8⁺ T cells, one leading to exhausted T cells and one leading to CD8⁺ T_{RMS} (figure 5F). The trajectory began with T4_CD8_naive T cells, followed by T6_CD8_central memory T cells, T1_CD8_effector T cells and

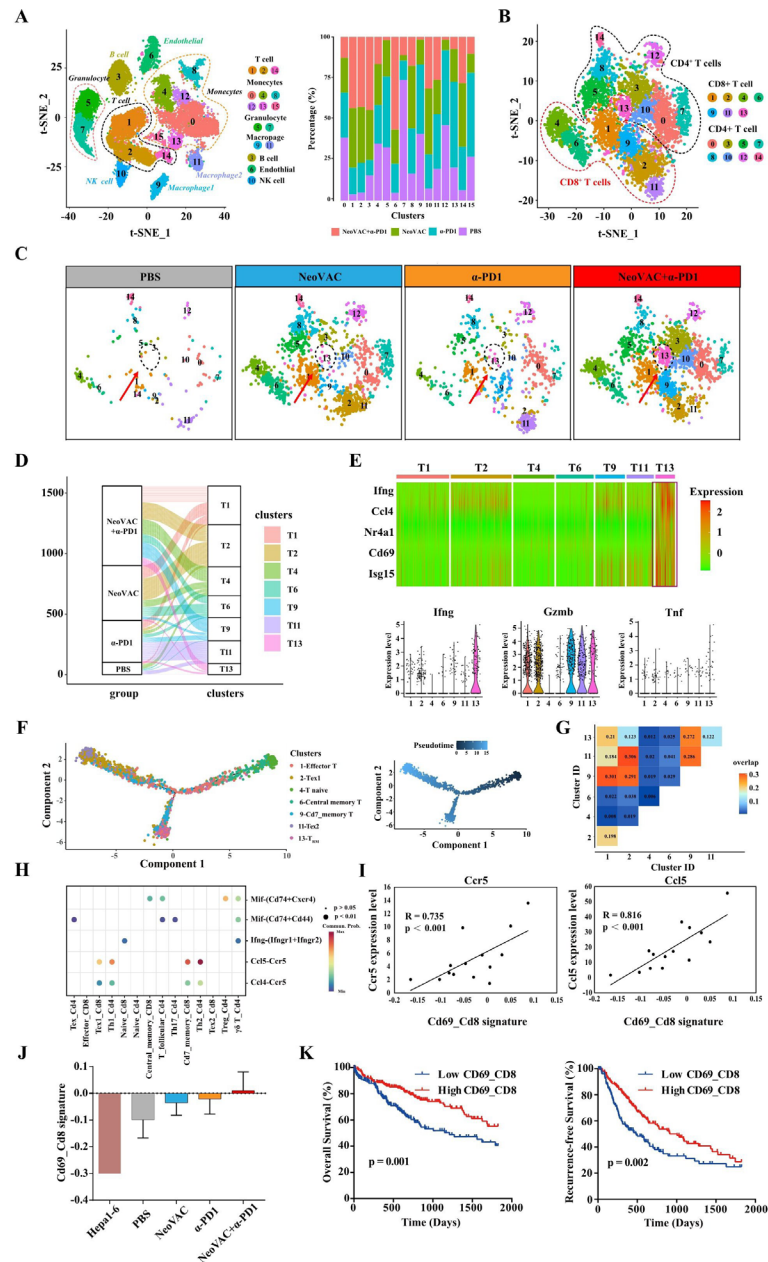


Figure 5 Characterization of mouse immune microenvironment via scRNA-seq and bulk RNA-seq data. (A) t-SNE plot showing CD45⁺ infiltrating cells merged from all groups (left); histogram indicating the proportion of clusters within each group (right). (B) t-SNE plot showing the subsets of infiltrating T-cell clusters. (C) t-SNE plots of infiltrating T cells separated by treatment condition, the arrow indicated the CD8⁺ T-cell cluster enriched in NeoVAC plus α -PD-1 group. (D) Alluvial plot connecting treatment groups and CD8⁺ T-cell clusters according to predicted TCR specificity. (E) Heatmap showing the expression of top upregulated genes of T13 cluster (top); expression levels of *Ifn-g*, *Gzmb*, *Tnf* across all CD8⁺ T-cell clusters (bottom). (F) Pseudotime trajectory of CD8⁺ T-cell clusters colored by clusters generated by Monocle 2 (left); Pseudotime trajectory of CD8⁺ T-cell clusters colored by pseudotime (dark blue to light blue) generated by Monocle 2 (right). (G) The overlap of TCR clonotypes between different CD8⁺ T-cell clusters. The number in each square indicating the overlap of clonotypes scaled to the length of unique clonotypes in the smaller sample. (H) Bubble chart showing the interactions between CD8⁺ T_{RM} subset and other T-cell subsets. The sizes of the bubbles indicate the significance of the interactions between different subsets and the color indicated the communication probability calculated by CellChat. (I) Scatterplot showing the correlation between the two-gene signature (*Cd69* and *Cd8a*) and *Ccr5* (right) or *Ccl5* (left) genes from T13 cluster. (J) Expression levels of CD8⁺ T_{RM} signature for different groups assessed by RNA-seq data, error bars represented SD for groups with replicates (n=4 for NeoVAC plus α -PD-1 group and NeoVAC only group; n=3 for α -PD-1 treated and PBS group). (K) Kaplan-Meier curves of 5-year overall survival (left) and recurrence-free survival (right) for patients with HCC from TCGA stratified by median expression level of two-gene signature (*CD69* and *CD8a*). t-SNE, t-distributed stochastic neighbor embedding. Survival curves were generated using Kaplan-Meier estimates and tested using the log-rank test. HCC, hepatocellular carcinoma; NeoVAC, neoantigen peptide vaccine; PBS, phosphate buffered saline; scRNA-seq, single-cell RNA sequencing; TCGA, The Cancer Genome Atlas; TCR, T-cell receptor; T_{RM}, tissue-resident memory T cells; α -PD-1, programmed cell death 1 blockade.

T9_CD8_Cd7 memory T cells. Then some T9_CD8_Cd7 memory T cells ended with exhausted T cells (T2_CD8_exhausted T cell1 and T11_CD8_exhausted T cell2), while some transformed into CD8⁺ T_{RM}s. Furthermore, TCR overlap analysis further confirmed that CD8⁺ T_{RM}s shared most TCRs with T9_CD8_Cd7 memory T cells, supporting that CD8⁺ T_{RM}s could indeed evolve from T9_CD8_Cd7 memory T cells (figure 5G). Moreover, ligand-receptor analysis revealed that T CD8⁺ T_{RM}s and Th2 cells have the highest communication probability via CCL5/CCR5 interaction, suggesting the recruitment of Th2 by CD8⁺ T_{RM}s might lead to better antitumor response (figure 5H). Consistently, the proportion of Th2 cells (T10) also increased in the tumor from NeoVAC plus α -PD-1 treated mouse (online supplemental figure S10A).

In addition, we also performed bulk RNA-seq of tumors isolated from different groups on day 12 after treatment. To acquire a gene signature representing the CD8⁺ T_{RM}s, we extracted the top 50, top 100 and top 200 upregulated genes of CD8⁺ T_{RM}s and evaluated their expression in tumor bulk RNA-seq data. Single-sample gene set enrichment analysis (ssGSEA) showed that a two-gene signature consisted of Cd69 and Cd8a had a significant positive correlation with CD8⁺ T_{RM}s' upregulated genes, suggesting it could well represent CD8⁺ T_{RM}s (online supplemental figure S10C). Intriguingly, the Cd69_Cd8a signature in bulk RNA-seq data showed a significant association with expression level of both Ccr5 and Ccl5, which is consistent with the results of ligand-receptor analysis (both $p < 0.001$, figure 5I). Furthermore, we observed the NeoVAC plus α -PD-1 treated group displaying highest expression of Cd69_Cd8a signature, while PBS group had the lowest expression level, which is consistent with the efficacy of immunotherapy (figure 5J). Meanwhile, the only mouse with recurrent tumor after rechallenge demonstrated low level of Cd69_Cd8a signature compared with PBS treated group, reflecting low level of CD8⁺ T_{RM}s in this tumor, which might explain the recurrence after rechallenge (data not shown). Kaplan-Meier's analysis of The Cancer Genome Atlas HCC data set further confirmed that the Cd69_Cd8a signature was a significant predictor of HCC prognosis, with tumors expressing higher Cd69_Cd8a signature showing significantly longer 5-year OS and recurrence-free survival rate ($p = 0.001$ and $p = 0.002$, respectively, figure 5K).

Validation of tumor-killing ability of CD8⁺ T_{RM}s for HCC treatment

Based on the findings aforementioned, we hypothesized that there would be more neoantigen-specific TILs in CD8⁺ T_{RM}s induced by our combinational therapy. To verify this hypothesis, flow cytometry analysis was performed in TILs collected from above mentioned four treated groups. Notably, as shown in figure 6A,B and online supplemental figure S11A, combinational therapy showed higher percentage of T_{RM}s in CD8⁺ T cells and higher percentage of Ptpn2-specific CD8⁺ T cells in CD8⁺ T_{RM}s than other three treated groups. These results further

confirmed the increased infiltration of CD8⁺ T_{RM}s after combinational therapy. Moreover, to investigate whether CD8⁺ T_{RM}s played a key role in tumor-killing, CD8⁺CD69⁺ and CD8⁺CD69⁻ TILs were isolated from combinational therapy mice by flow cytometry sorting and subsequently co-cultured with Hepa1-6 cells for 48 hours, respectively (figure 6C). Then the tumor-killing ability and cytokine secretion were analyzed by flow cytometry and ELISA arrays, respectively. Interestingly, higher amounts of apoptotic cells and higher IFN- γ /tumor necrosis factor (TNF)- α secretion were observed in CD8⁺CD69⁺ TILs coincubated group than CD8⁺CD69⁻ TILs coincubated group (figure 6D-F). Furthermore, we evaluated the tumor-killing ability of CD8⁺CD69⁺ TILs in orthotopic HCC models. As shown in figure 6G, CD8⁺CD69⁺ and CD8⁺CD69⁻ TILs sorted from tumors treated by NeoVAC plus α -PD-1 were injected into orthotopic HCC mice via tail vein ($n = 4$) and further injected IL-2 for five consecutive days, respectively (mice injected with IL-2 were served as the control group, $n = 4$). Expectedly, mice injected with CD8⁺CD69⁺ TILs experienced significantly lower tumor burden than control or CD8⁺CD69⁻ TILs treated groups (figure 6H and online supplemental figure S11B). The results illustrated that CD8⁺ T_{RM}s may be crucial for tumor-killing both in vitro and in vivo. To further confirm these findings in patients with HCC, CD8⁺CD69⁺ and CD8⁺CD69⁻ TILs from surgically removed patients' HCC fresh tumor samples were sorted and then co-cultured with autologous patient-derived cells (PDCs) for 48 hours (figure 6J). Noteworthy, Flow cytometry analysis showed that CD8⁺CD69⁺ TILs induced more apoptosis of PDCs when compared with CD8⁺CD69⁻ TILs (figure 6J), which provided strong supporting evidence for the pivotal role of CD8⁺ T_{RM}s in tumor-killing.

DISCUSSION

NeoVAC has been proved as a promising antitumor immunotherapy strategy in several solid tumors with high tumor mutation burden, but still needs to be deeply explored in HCC.^{3,36} In this study, we first demonstrated that when compared with the addition of other TLRs agonists as adjuvant, NeoVAC composed of Hepa1-6 personalized neoantigen peptides and TLR3 agonist Poly(I:C) adjuvant could induce significantly stronger antitumor immune response in mice for HCC treatment. However, we also found that neoantigen-specific T cells induced by NeoVAC alone expressed high level of PD-1, which was prone to exhaustion in the HCC immunosuppressive microenvironment. Significantly, when combined with the immune checkpoint inhibitor PD-1 antibody, the neoantigen-specific antitumor immune response induced by the NeoVAC can be significantly enhanced. Meanwhile, in orthotopic HCC model for treatment or in the orthotopic recurrence and metastasis HCC model, this combinational therapy also shows excellent synergistic antitumor killing ability and long-term tumor-specific immunological memory, which might be

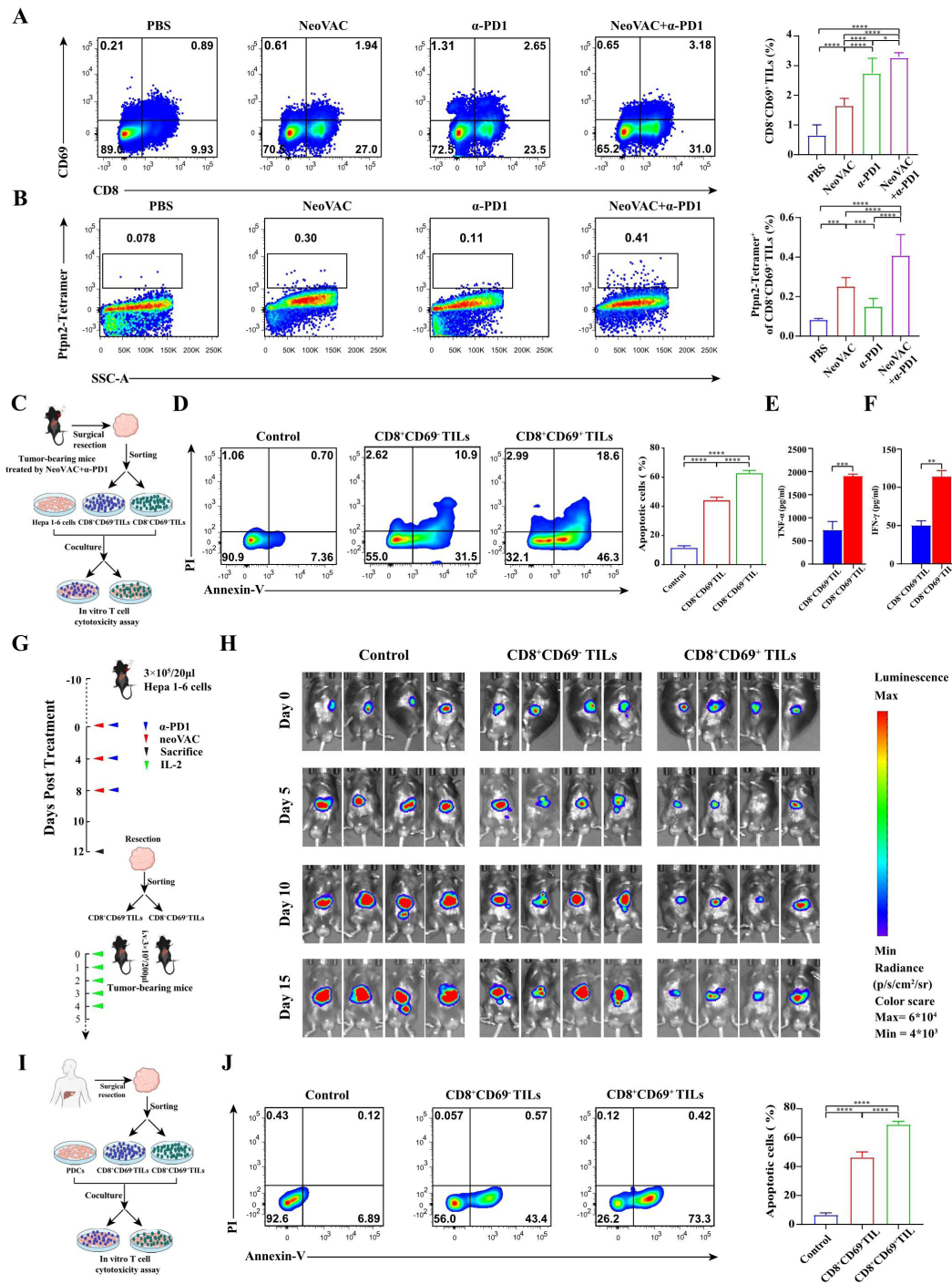


Figure 6 Infiltration and antitumor efficacy of CD8⁺ T_{RMs}. (A) Flow cytometry analysis showing the percentage of CD8⁺ T_{RMs} in infiltrating CD8⁺ T cells of PBS, NeoVAC alone, α-PD-1 alone and NeoVAC plus α-PD-1 treated groups (n=5). (B) Flow cytometry analysis showing the percentage of Ptpn2³⁷⁶⁻³⁸⁴:H-2K^b specific CD8⁺ T cells in infiltrating CD8⁺ T_{RMs} (n=5). (C) Schematic diagram of in vitro tumor-killing efficacy evaluation of CD8⁺CD69⁺ and CD8⁺CD69⁻ T cells isolated from Hepa1-6 tumor tissues after combined treatment. (D) Flow cytometry showing the percentage of apoptotic cells induced by CD8⁺CD69⁺ or CD8⁺CD69⁻ TILs (n=3). (E) ELISA assay showing secretion of TNF-α from CD8⁺CD69⁺ or CD8⁺CD69⁻ TILs (n=3). (F) ELISA assay showing secretion of IFN-γ from CD8⁺CD69⁺ or CD8⁺CD69⁻ TILs (n=3). (G) Schematic diagram of adoptive CD8⁺CD69⁺ or CD8⁺CD69⁻ T cells therapy in orthotopic HCC mouse models. (H) Tumor burden monitoring of mice after adoptive CD8⁺CD69⁺ or CD8⁺CD69⁻ T cells therapy by bioluminescence imaging (n=4). (I) Schematic diagram of in vitro tumor-killing efficacy evaluation of CD8⁺CD69⁺ and CD8⁺CD69⁻ T cells isolated from patient's tumor tissue. (J) Flow cytometry analysis showing the percentage of apoptotic cells induced by CD8⁺CD69⁺ or CD8⁺CD69⁻ TILs in PDCs (n=6). Ptpn2, Ptpn2³⁷⁶⁻³⁸⁴:H-2K^b. The statistical analysis was performed with analysis of variance analysis. Results are shown as mean±SD. *p<0.05; **p<0.01; ***p<0.001; ****p<0.0001. HCC, hepatocellular carcinoma; IFN, interferon; IL, interleukin; NeoVAC, neoantigen peptide vaccine; PDCs, patient-derived cells; TIL, tumor infiltrating lymphocytes; TNF, tumor necrosis factor; T_{RMs}, tissue-resident memory T cells; α-PD-1, programmed cell death 1 blockade.

an effective treatment in other solid tumors for clinical translation.²⁰

CD8⁺ T cells are the major component of TILs and mediate innate and adaptive immune responses to hepatitis B virus (HBV), neoantigen, tumor-associated, and disease-unrelated antigens in HCC.^{39–40} Among them, CD8⁺ T_{RM}s, expressed CD69 in cell surface, have been proven as key effector cells against solid tumors including HCC.^{41–42} Recent large-scale mass cytometry and scRNA-seq on T cells from HCC tissue showed that HBV or neoantigen-specific CD8⁺ T_{RM}s could enrich in HBV-related HCC and significantly correlate with long-term recurrence-free survival of patients with HCC.³⁹ However, this T-cell subset often had high PD-1 expression and showed suppressive and exhausted status in HCC micro-environment.⁴⁰ Therefore, how to successfully recruit and reactivate CD8⁺ T_{RM}s in HCC is the key to HCC immunotherapy. More significantly, in this study, we found that CD8⁺ T_{RM}s derived from effector memory T cells/Cd7_{memory} T cells could significantly enrich in HCC tissue by the combinational treatment of NeoVAC and α-PD-1. Meanwhile, these T cells contained a relatively higher proportion of neoantigen-specific T cells and showed higher activation activity and higher secretion of tumor-killing-related cytokines than other CD8 T cells. Both in vitro and in vivo mouse HCC models or patient HCC PDC models have verified the powerful tumor-killing ability of CD8⁺ T_{RM}s. Furthermore, bulk RNA-seq has revealed the detailed mechanism of CD8⁺ T_{RM}s elicited significant antitumor efficacy. Overall, our results provide compelling evidence to support a central role for CD8⁺ T_{RM}s in antitumor immunity, and indicate that CD8⁺ T_{RM}s could serve as a robust immunotherapeutic target for HCC.

Furthermore, several reports also indicate that in addition to their well-documented direct tumor-killing capability, CD8⁺ T_{RM}s could also activate cross-presenting dermal DCs and subsequently further prime and expand new CD8⁺ T cells for responding to tumor-derived neoantigens and self-antigens.^{43–44} However, whether CD8⁺ T_{RM}s also have such related versatility in HCC remains to be further analyzed. Herein, we have provided some potential evidence to support the multifunction of CD8⁺ T_{RM}s in HCC through single cell and bulk sequencing data. First, large amounts of effector cytokines (such as IFN-γ and TNF-α) secreted by CD8⁺ T_{RM}s could activate other immune cells with antitumor potential. Second, CD8⁺ T_{RM}s also highly express several chemokines including CCL4 and CCL5, which could recruit Th2 and Cd7_{memory} T cells in HCC tissue to enhance antitumor immune response. Accordingly, these data suggested CD8⁺ T_{RM}s might cooperate with other T cells to support antitumor immunity for HCC.

In summary, we showed that NeoVAC plus α-PD-1 could induce powerful antitumor effect and long-term tumor-specific immune memory in HCC model by remodeling the immunosuppressive TME. Moreover, CD8⁺ T_{RM}s were found to be significantly increased in HCC tissues after combinational treatment, which contained a relatively high proportion of neoantigen-specific T cells and significantly related

to the antitumor efficacy. Overall, this concept provided a new insight for boosting the number and ability of CD8⁺ T_{RM}s to enhance antitumor immunity in patients with advanced HCC. However, due to the limited HCC models used in this study, the corresponding findings still need to be further validated in other HCC animal models and clinical trials.

Author affiliations

¹The United Innovation of Mengchao Hepatobiliary Technology Key Laboratory of Fujian Province, Mengchao Hepatobiliary Hospital of Fujian Medical University, Fuzhou, China

²The Liver Center of Fujian Province, Fujian Medical University, Fuzhou, China

³Mengchao Med-X Center, Fuzhou University, Fuzhou, China

⁴Department of Colorectal Surgery, The First Affiliated Hospital of Fujian Medical University, Fuzhou, China

Acknowledgements The authors would like to thank Fujian Provincial Clinical Research Center for Hepatobiliary and Pancreatic Tumors (2020Y2013) for assistance. The results shown here are part based upon data generated by the TCGA Research Network: <https://www.cancer.gov/tcga>.

Contributors Conception and design: ZC and XL. Development of methodology: HC, ZL, LQ, GC, XD, YS and JO. Acquisition of Data: HC, XD, LC, WL, YZ and HY. Analysis and interpretation of data: HC, ZL, ZC and XL. Writing, review, and/or revision of the manuscript: HC, ZL, ZC and XL. Study Supervision: ZC and XL. XL is responsible for the overall content as guarantor.

Funding This work was supported by Joint funds for the Innovation of science and technology of Fujian province (Grant Number 2020Y9044), scientific foundation of Fujian province (Grant Number 2022J011280 and 2020J011171), Young and middle aged talent training project of Fujian provincial health commission (Grant Number 2021GGA066), Fuzhou science and technology planning project (Grant Number 2021-S-113) and Startup fund for scientific research, Fujian medical university (Grant Number: 2019QH2032), Fuzhou "14th Five-Year" clinical key specialty (Grant Number: 20220203).

Competing interests None declared.

Patient consent for publication Not applicable.

Ethics approval Institutional review board—approved written and informed consent was obtained from patients with hepatocellular carcinoma to obtain tumor tissues for analysis. All studies were performed in accordance with ethical regulations and approved by the Ethics Review Committee of Mengchao Hepatobiliary Hospital of Fujian Medical University (KESHEN 2021_110_01). All animal procedures were approved by the Animal Ethics Committee of Mengchao Hepatobiliary Hospital of Fujian Medical University (2021-8CAARM177).

Provenance and peer review Not commissioned; externally peer reviewed.

Data availability statement Data are available in a public, open access repository. The raw sequencing data in this article has been deposited at Genome Sequencing Archive database (GSA, <https://hgdc.cnbc.ac.cn/gsa>) under the accession number of CRA006378.

Supplemental material This content has been supplied by the author(s). It has not been vetted by BMJ Publishing Group Limited (BMJ) and may not have been peer-reviewed. Any opinions or recommendations discussed are solely those of the author(s) and are not endorsed by BMJ. BMJ disclaims all liability and responsibility arising from any reliance placed on the content. Where the content includes any translated material, BMJ does not warrant the accuracy and reliability of the translations (including but not limited to local regulations, clinical guidelines, terminology, drug names and drug dosages), and is not responsible for any error and/or omissions arising from translation and adaptation or otherwise.

Open access This is an open access article distributed in accordance with the Creative Commons Attribution Non Commercial (CC BY-NC 4.0) license, which permits others to distribute, remix, adapt, build upon this work non-commercially, and license their derivative works on different terms, provided the original work is properly cited, appropriate credit is given, any changes made indicated, and the use is non-commercial. See <http://creativecommons.org/licenses/by-nc/4.0/>.

ORCID iD

Xiaolong Liu <http://orcid.org/0000-0002-3096-4981>

REFERENCES

- 1 Siegel RL, Miller KD, Fuchs HE, et al. Cancer statistics, 2021. *CA Cancer J Clin* 2021;71:7–33.
- 2 Qiu Z, Li H, Zhang Z, et al. A pharmacogenomic landscape in human liver cancers. *Cancer Cell* 2019;36:e11:179–93.
- 3 Sangro B, Sarobe P, Hervás-Stubbs S, et al. Advances in immunotherapy for hepatocellular carcinoma. *Nat Rev Gastroenterol Hepatol* 2021;18:525–43.
- 4 Hu Z, Ott PA, Wu CJ. Towards personalized, tumour-specific, therapeutic vaccines for cancer. *Nat Rev Immunol* 2018;18:168–82.
- 5 Hilf N, Kuttruff-Coqui S, Frenzel K, et al. Actively personalized vaccination trial for newly diagnosed glioblastoma. *Nature* 2019;565:240–5.
- 6 Schumacher TN, Schreiber RD. Neoantigens in cancer immunotherapy. *Science* 2015;348:69–74.
- 7 Carreno BM, Magrini V, Becker-Hapak M, et al. Cancer immunotherapy. A dendritic cell vaccine increases the breadth and diversity of melanoma neoantigen-specific T cells. *Science* 2015;348:803–8.
- 8 Keskin DB, Anandappa AJ, Sun J, et al. Neoantigen vaccine generates intratumoral T cell responses in phase Ib glioblastoma trial. *Nature* 2019;565:234–9.
- 9 Sahin U, Derhovanesian E, Miller M, et al. Personalized RNA mutanome vaccines mobilize poly-specific therapeutic immunity against cancer. *Nature* 2017;547:222–6.
- 10 Ott PA, Hu Z, Keskin DB, et al. An immunogenic personal neoantigen vaccine for patients with melanoma. *Nature* 2017;547:217–21.
- 11 Lu F, Ma X-J-N, Jin W-L, et al. Neoantigen specific T cells derived from T cell-derived induced pluripotent stem cells for the treatment of hepatocellular carcinoma: potential and challenges. *Front Immunol* 2021;12:690565.
- 12 Li Z, Chen G, Cai Z, et al. Profiling of hepatocellular carcinoma neoantigens reveals immune microenvironment and clonal evolution related patterns. *Chin J Cancer Res* 2021;33:364–78.
- 13 Cai Z, Su X, Qiu L, et al. Personalized neoantigen vaccine prevents postoperative recurrence in hepatocellular carcinoma patients with vascular invasion. *Mol Cancer* 2021;20:164.
- 14 Tumei PC, Harview CL, Yearley JH, et al. PD-1 blockade induces responses by inhibiting adaptive immune resistance. *Nature* 2014;515:568–71.
- 15 Yau T, Kang Y-K, Kim T-Y, et al. Efficacy and safety of nivolumab plus ipilimumab in patients with advanced hepatocellular carcinoma previously treated with sorafenib: the CheckMate 040 randomized clinical trial. *JAMA Oncol* 2020;6:e204564.
- 16 Kelley RK, Sangro B, Harris WP, et al. Efficacy, tolerability, and biologic activity of a novel regimen of tremelimumab (T) in combination with durvalumab (D) for patients (PTS) with advanced hepatocellular carcinoma (aHCC). *J Clin Oncol* 2020;38:4508.
- 17 Finn RS, Qin S, Ikeda M, et al. Atezolizumab plus bevacizumab in unresectable hepatocellular carcinoma. *N Engl J Med* 2020;382:1894–905.
- 18 Finn RS, Ikeda M, Zhu AX, et al. Phase Ib study of lenvatinib plus pembrolizumab in patients with unresectable hepatocellular carcinoma. *J Clin Oncol* 2020;38:2960–70.
- 19 Hu Z, Leet DE, Allesøe RL, et al. Personal neoantigen vaccines induce persistent memory T cell responses and epitope spreading in patients with melanoma. *Nat Med* 2021;27:515–25.
- 20 Ott PA, Hu-Lieskovan S, Chmielowski B, et al. A phase Ib trial of personalized neoantigen therapy plus anti-PD-1 in patients with advanced melanoma, non-small cell lung cancer, or bladder cancer. *Cell* 2020;183:347–62.
- 21 Koboldt DC, Chen K, Wylie T, et al. VarScan: variant detection in massively parallel sequencing of individual and pooled samples. *Bioinformatics* 2009;25:2283–5.
- 22 Chang X, Wang K. wANNOVAR: annotating genetic variants for personal genomes via the web. *J Med Genet* 2012;49:433–6.
- 23 Jurtz V, Paul S, Andreatta M, et al. NetMHCpan-4.0: improved peptide-MHC class I interaction predictions integrating eluted ligand and peptide binding affinity data. *J Immunol* 2017;199:3360–8.
- 24 Satija R, Farrell JA, Gennert D, et al. Spatial reconstruction of single-cell gene expression data. *Nat Biotechnol* 2015;33:495–502.
- 25 Aran D, Looney AP, Liu L, et al. Reference-based analysis of lung single-cell sequencing reveals a transitional profibrotic macrophage. *Nat Immunol* 2019;20:163–72.
- 26 Heng TS, Painter MW. Immunological genome project C. The immunological genome Project: networks of gene expression in immune cells. *Nat Immunol* 2008;9:1091–4.
- 27 Lee S-K, Chwee JY, Ma CAP, et al. Synergistic anticancer effects of Pam3CSK4 and Ara-C on B-cell lymphoma cells. *Clin Cancer Res* 2014;20:3485–95.
- 28 Vacchelli E, Martins I, Eggermont A, et al. Trial watch: peptide vaccines in cancer therapy. *Oncology* 2012;1:1557–76.
- 29 Cluff CW. Monophosphoryl lipid A (MPL) as an adjuvant for anti-cancer vaccines: clinical results. *Adv Exp Med Biol* 2010;667:111–23.
- 30 Stahl-Hennig C, Eisenblätter M, Jasny E, et al. Synthetic double-stranded RNAs are adjuvants for the induction of T helper 1 and humoral immune responses to human papillomavirus in rhesus macaques. *PLoS Pathog* 2009;5:e1000373.
- 31 Asprodites N, Zheng L, Geng D, et al. Engagement of toll-like receptor-2 on cytotoxic T-lymphocytes occurs in vivo and augments antitumor activity. *Faseb J* 2008;22:3628–37.
- 32 Ingale S, Wolfert MA, Gaekwad J, et al. Robust immune responses elicited by a fully synthetic three-component vaccine. *Nat Chem Biol* 2007;3:663–7.
- 33 Salem ML, El-Naggar SA, Kadima A, et al. The adjuvant effects of the toll-like receptor 3 ligand polyinosinic-cytidylic acid poly (I:C) on antigen-specific CD8+ T cell responses are partially dependent on NK cells with the induction of a beneficial cytokine milieu. *Vaccine* 2006;24:5119–32.
- 34 Krieg AM. Therapeutic potential of toll-like receptor 9 activation. *Nat Rev Drug Discov* 2006;5:471–84.
- 35 Neidhart J, Allen KO, Barlow DL, et al. Immunization of colorectal cancer patients with recombinant baculovirus-derived KSA (Ep-CAM) formulated with monophosphoryl lipid A in liposomal emulsion, with and without granulocyte-macrophage colony-stimulating factor. *Vaccine* 2004;22:773–80.
- 36 Mellman I, Steinman RM. Dendritic cells: specialized and regulated antigen processing machines. *Cell* 2001;106:255–8.
- 37 Bartsch LM, Damasio MPS, Subudhi S, et al. Tissue-resident memory T cells in the liver-unique characteristics of local specialists. *Cells* 2020;9:9112457:2457. doi:10.3390/cells9112457
- 38 Park SL, Gebhardt T, Mackay LK. Tissue-resident memory T cells in cancer immunosurveillance. *Trends Immunol* 2019;40:735–47.
- 39 Cheng Y, Gunasegaran B, Singh HD, et al. Non-terminally exhausted tumor-resident memory HBV-specific T cell responses correlate with relapse-free survival in hepatocellular carcinoma. *Immunity* 2021;54:1825–40.
- 40 Lim CJ, Lee YH, Pan L, et al. Multidimensional analyses reveal distinct immune microenvironment in hepatitis B virus-related hepatocellular carcinoma. *Gut* 2019;68:916–27.
- 41 Snyder ME, Finlayson MO, Connors TJ, et al. Generation and persistence of human tissue-resident memory T cells in lung transplantation. *Sci Immunol* 2019;4:5581. doi:10.1126/sciimmunol.aav5581
- 42 Menares E, Gálvez-Cancino F, Cáceres-Morgado P, et al. Tissue-resident memory CD8+ T cells amplify anti-tumor immunity by triggering antigen spreading through dendritic cells. *Nat Commun* 2019;10:4401.
- 43 Nizard M, Roussel H, Diniz MO, et al. Induction of resident memory T cells enhances the efficacy of cancer vaccine. *Nat Commun* 2017;8:15221.
- 44 Mueller SN, Mackay LK. Tissue-resident memory T cells: local specialists in immune defence. *Nat Rev Immunol* 2016;16:79–89.